Entanglement Capacity Estimates and Throughput Measurements of Quantum Channels

Nageswara S. V. Rao
Computational Sciences and Engineering Division
Oak Ridge National Laboratory
Oak Ridge, USA
raons@ornl.gov

Muneer Alshowkan
Computational Sciences and Engineering Division
Oak Ridge National Laboratory
Oak Ridge, USA
alshowkanm@ornl.gov

Joseph C. Chapman
Computational Sciences and Engineering Division
Oak Ridge National Laboratory
Oak Ridge, USA
chapmanjc@ornl.gov

Nicholas A. Peters
Computational Sciences and Engineering Division
Oak Ridge National Laboratory
Oak Ridge, USA
petersna@ornl.gov

Hsuan-Hao Lu
Computational Sciences and Engineering Division
Oak Ridge National Laboratory
Oak Ridge, USA
luo2@ornl.gov

Joseph M. Lukens
Research Technology Office
Arizona State University
Tempe, AZ, USA
Joseph.Lukens@asu.edu

Saikat Guha
Department of Electrical and Computer Engineering
University of Maryland
College Park, MD, USA
saikat@umd.edu

***Abstract*—The throughput is an important performance metric of entangled qubit distribution quantum networks, and may be characterized by the number of distributed entangled qubit pairs per second (ebps). It is measured over physical quantum network connections using specialized instruments, including photonic entanglement sources and single photon detectors. Extensive theory has been developed to estimate the entangled qubit capacity of quantum channels using abstractions of physical connections. These two quantities both characterize the throughput performance but in different ways, and typically have been hard to relate to each other in concrete terms, in part due to the lack of precise measurements with matching analytical models and derivations. We describe measurements on a physical testbed with fiber connections of lengths 0-75 kilometers. We obtain the normalized analytic capacity estimates using the transmissivity approximations derived using single photon coincidence measurements, and convert them to bounds on throughput (measured in ebps) using a multiplier derived from co-located detector measurements. The results indicate consistent throughput measurements upper-bounded by their analytical capacity estimates across all connections. We show that previous capacity estimates using light measurements are below ebps measurements for some connections, due to the inclusion of non-representative decrease of light levels outside C-band with distance.**

***Index Terms*—ebit, entangled bits per second, throughput estimates, channel capacity, quantum network testbed**

This research is sponsored in part by Entanglement Distribution and PiQSci projects of Advanced Scientific Computing Research program, U.S. Department of Energy, and is performed at Oak Ridge National Laboratory managed by UT-Battelle, LLC for U.S. Department of Energy under Contract No. DE-AC05-00OR22725. This manuscript has been co-authored by UT-Battelle, LLC, under contract DE-AC05-00OR22725 with the US Department of Energy (DOE). The US government retains and the publisher, by accepting the article for publication, acknowledges that the US government retains a nonexclusive, paid-up, irrevocable, worldwide license to publish or reproduce the published form of this manuscript, or allow others to do so, for US government purposes. DOE will provide public access to these results of federally sponsored research in accordance with the DOE Public Access Plan (http://energy.gov/downloads/doe-public-access-plan).

I. Introduction

The throughput of entanglement distribution is an important performance metric of quantum networks. In conventional networks, throughput is normally characterized in terms of the number of distributed bits per second (bps), and has been extensively studied and utilized in practical network designs [1]. While there are several throughput performance metrics in quantum networks based on quantum bits (qubits), entangled qubits (ebits), and secret-key bits (sbits) [2], the ebits per second (ebps) is important due its vital role as a required resource for quantum teleportation [3]. The ebps measurements over fiber connections require specialized (imperfect, even if calibrated) equipment, for example, photonic entanglement

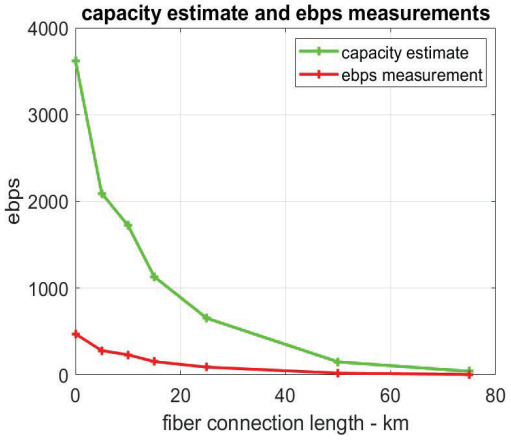

(a) linear scale

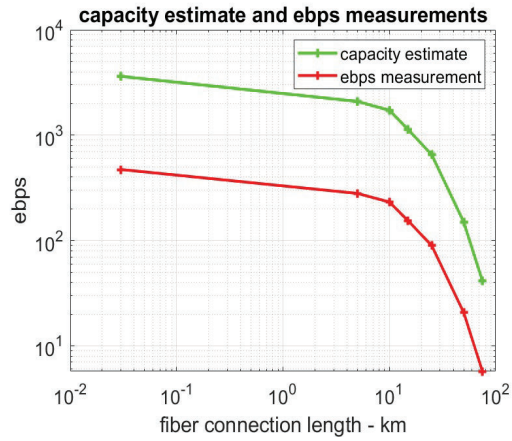

(b) log-log scale

Fig. 1: Capacity estimates and entanglement throughput measured in ebps over 0-75km connections in linear and log-log scales.

sources and superconducting nanowire single-photon detectors (SNSPDs) [4]. In term of theory, methods have been developed to estimate the capacity of quantum connections by modeling them as generic quantum channels [3]. These capacity estimates are specialized for fiber connections by using the *transmissivity* as a key parameter [5], which provide upper bounds on achievable throughput. In addition, they also offer qualitative insight on the dependence of ebps throughput on the connection properties such as length and loss. In practice, however, ebps measurements and the analytical capacity estimates often have been hard to correlate in part due to the lack of precise measurements with well-characterized analytic models. In this paper, we present a systematic study of entanglement throughput (ebps) measured over physical fiber connections, and the corresponding analytical capacity estimates, both for quantum repeater-less optical connections [5].

The measured ebps throughput depends on a variety of factors including connection length, fiber quality, detector efficiency and others, and we focus on the connection length with other parameters remaining fixed. We collect ebps measurements over physical fiber connections of variable lengths

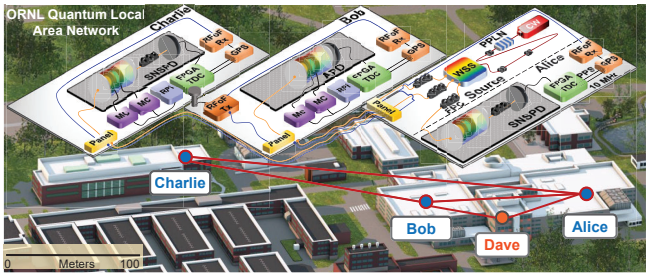

Fig. 2: Quantum Network (QNET) testbed with nodes named Alice, Bob, Charlie, and Dave with quantum node configurations shown as insets. The acronyms and labels are described in Table I.

10 MHz	reference clock
APD	avalanche photo diode
AWG	arbitrary waveform generator
CW	continuous-wave laser
FPC	fiber polarization controller
FPGA	field-programmable gate array
GPS	Global Positioning System
Panel	fiber-optic patch panel
PPLN	periodically poled lithium niobate
PPS	pulse per second
Source	entanglement source
RFoF Rx	RF over fiber receiver
RFoF Tx	RF over fiber transmitter
RPi	Raspberry Pi board (to control MCs)
SNSPD	superconducting nanowire single-photon detector.
TDC	time-to-digital converter
WSS	wavelength-selective switch

TABLE I: Acronyms and labels of devices deployed in QNET using naming convention in [6].

of 0-75 km and estimate the corresponding capacities, as summarized in Fig. 1. We utilize the two-photon coincidence measurements from SNSPDs to estimate the transmissivity parameter used in the capacity estimate, which is normalized to a single transmission attempt. We convert this normalized capacity to a bound on ebps by multiplying with the entangled source emission rate estimated using coincidence measurements collected using a pair of SNSPDs. The results indicate the consistency of ebps measurements and the corresponding capacity upper-bounds across all connections, as shown in Fig. 1. All measurements are collected on the quantum network (QNET) [4] at the Department of Energy's Oak Ridge National Laboratory (ORNL) shown in Fig. 2 [7].

In previous studies, light intensities over these connections have been measured and used in analytical formulae [5] to derive the normalized capacity estimates [7]. We show here that these capacity estimates may appear inconsistent since they are lower than ebps measurements for some connections. Our results indicate that these capacity estimates decrease

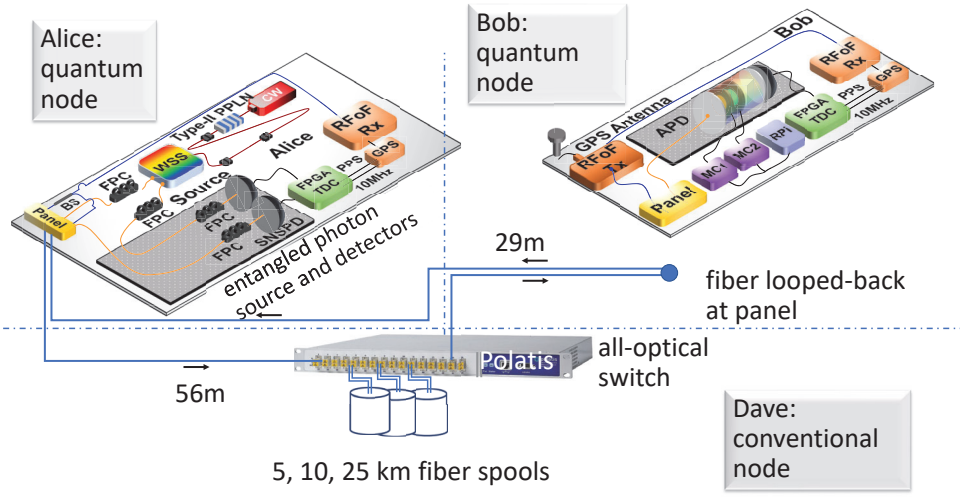

Fig. 3: Fiber spools are selected to provision a connection of 0-75km length under ORNL QNET telescopic design using an all-optical Polatis switch [4]. The acronyms and labels are described in Table I.

faster with distance compared to C-band entangled photons corresponding to ebps measurements.

The organization of this paper is as follows. The QNET testbed [4] and configurations used for measurements are described in Section II. The ebps and other measurements are described in Section III. The normalized capacity estimates for single channel use are described in Section IV, and they converted to bounds on achievable throughput in ebps which are compared with measurements in Section V. The conclusions and future directions are described in Section VI.

II. QNET Testbed with Fiber Spool Telescoping

The QNET testbed [2], [4], [6], [8], shown in Fig. 2, is configurable with six fiber spools to provide a suite of connections with increasing length to support scaling tests [7]. The quantum node Alice and the conventional node Dave, shown in Fig. 3, are utilized in realizing these connections one at a time for collecting ebps throughput measurements. The two-photon entangled source and two SNSPDs are located at the Alice node, and the connections are routed through the Bob and Dave nodes. The fiber is patched at the panel at node Bob and is connected via a transparent all-optical switch (Polatis) at node Dave, where a subset of fiber spools are chosen to compose a connection of specific length. Both ends of each fiber spool are connected to the Polatis switch, and those of selected spools are cross-connected to form a sub-connection whose ends are connected to fiber connections to nodes Alice and Bob. Thus, each connection originates at Alice, includes select set of fiber spools in Dave, passes through Bob, and returns to Alice, as shown in Fig. 3. At node Alice, the entanglement source is connected to two SNSPDs such that one entangled photon traverses the local fiber connection while the other traverses the connection provisioned through the Polatis switch and node Bob.

Three 25 km, one 10 km, one 5 km, and twelve 30 m single-mode fiber spools are attached to an all-optical switch at both

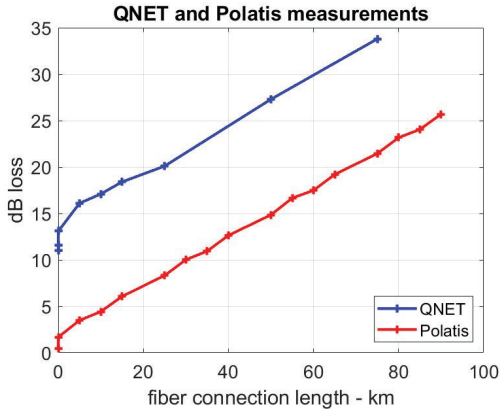

Fig. 4: Optical power loss measurements collected on the Polatis switch, and at the QNET node Alice are used to estimate losses of connections in dB.

ends. They are configured in a telescoping scheme by choosing and cross-connecting a subset of fibers on an all-optical switch to realize distances of 30 m as well as 5, 10, 15, 25, 30, 35, 40, 50, 55, 60, 65 and 75 km. These spool-connections are provisioned one at a time, and their power levels are measured at input and output ends on the switch.

The experimental setup in [4], [8] is used for measureing the entangled throughput in ebps, wherein the polarization-entangled photon source at Alice is composed of a 10-mm-long, periodically poled lithium niobate (PPLN) waveguide (HC Photonics), phasematched for type-II spontaneous parametric down-conversion (SPDC). The entanglement distribution starts from the source in the quantum lab at node Alice. While one photon is measured at Alice, the other is sent to the all-optical switch through several fiber spools, then sent to Bob's patch panel, where it is looped back to Alice for coincidence detection using SNSPDs (Quantum Opus). Components of the polarization analyzer include a quarter-

wave plate (QWP), half-wave plate (HWP), and polarizing beam splitter (PBS) followed by the SNSPDs for polarization state tomography and coincidence measurement. After the polarization analyzers, the detectors are preceded by fiber polarization controllers (FPCs) to maximize the polarization-dependent detection efficiency of the SNSPDs.

III. Measurement Collection

The entangled throughput measurements and the corresponding estimated capacity using coincidence measurements on SNSPDs provide complementary information about the achievable rates over the deployed quantum networks. The expectation is that entangled throughput measurements are below the capacity estimates which represent the maximum achievable throughput.

A. Entangled Throughput Measurements

We estimate the entanglement throughput rate by utilizing the single photon detections at two SNSPDs at Alice node in a post-processing step. By accounting for the connection latency, two detections within a time window of 1 nano second are counted as a single entanglement distribution event. This estimation is a reasonable approximation for the task at hand, as the QNET measured fidelities $> 90\%$ for this entangled photon source [8]. This high fidelity level suggests that the coincident detections are highly likely the result of entangled photons registered at their respective detectors, while the probability of accidental coincidences caused by noise or spurious photons is exceedingly low. These measurements decrease with the connection length as shown in Fig. 1a; its profile is convex in sharp contrast with the concave profile of conventional throughput measurements (in bps) collected using iperf in [7].

B. Entangled Photon Source Emission Rate Measurements

The emission rate of entangled photons at the source S_e is needed to convert the (normalized) capacity estimates provided by theory [3], [5] into those for throughput in ebps. This rate is measured using two co-located SNSPDs in node Alice, wherein they are directly connected to the two output ports of a WSS, each carrying one of the two entangled photons, as shown in Fig. 6. In this configuration, both paths are of nearly equal length, and are entirely local to node Alice; in particular, the QNET is disconnected during these measurements.

C. Signal Power Measurements

To facilitate a comparison with previous studies based on light level measurements, we briefly describe the configurations in [7]. For each connection, the light levels (dBm) are measured on Polatis switch, and additionally at the source and two SNSPDs in node Alice, as shown in Fig. 4 as a function of the connection length in km. In addition to losses in the fiber spools and Polatis cross-connects, there are additional losses on the end-to-end connection from source through destination; there are losses at the Alice node due to source collection and detection efficiency, and during the propagation from the quantum nodes to conventional node and back. The connection loss values (in dB) are derived from measurements, which show an additional 15–20 dB loss for the end-to-end connections compared to sub-connections on the Polatis switch, in part due to the fiber connections between the Polatis and node Alice, both direct and via node Bob.

IV. Capacity Estimates Per Channel Use

A generic analytical model of a quantum communications channel is specified by a linear, completely positive, trace preserving map that captures the corresponding quantum physical evolution [3]. It takes a particular form under the Choi–Kraus decomposition, expressed in terms of Kraus operators. Several types of quantum capacity are defined for quantum channels under various parametrizations, for example, dephasing and depolarizing [9]. Such channel models are inferred by process tomography using measurements collected on QNET [9]. By modeling an optical fiber connection as a quantum channel, analytical capacity estimates are derived in terms of the transmissivity parameter [3]. We consider a specific simplified optical channel without quantum repeaters which is characterized by the transmissivity parameter based on total loss [5].

For a fiber optical quantum communications connection, the entanglement capacity estimate per channel use is derived in [5] as

$$D_2(\eta) = -\log_2(1-\eta),$$

where η is the transmissivity of the optical channel specific to the entangled photon transmission. It provides a bound on throughput in ebits transmitted in a single channel use when one entangled photon of a pair is sent. When multiplied by the source entangled photon rate S_e, it provides a bound on the channel ebps rate R_e such that $S_e D_2(\eta) \geq R_e$. Here, η is a function of the connection length l, which typically results in a convex capacity that decays faster than linear as a function of l. The transmissivity in this case is given by a fraction of entangled source photons that are successfully transmitted through the connection to those sent from the source within a fixed time interval.

A. Transmissivity using Coincidence Measurements

The coincidence measurements of a connection are used to approximate its transmissivity η_c as explained next. The loopback fiber connection at node Alice corresponds to a QNET connection of (nearly) zero length, and its ebps measurements are subject to (nearly) zero loss. The transmissivity η_c of a connection is obtained by dividing its ebps measurements by those of the loopback connection. The first ebps measurements correspond to C-band (1560-nm) photons that successfully traversed through the connection and latter to those measured within Alice node with no QNET connection, and thus their ratio represents the transmissivity η of the connection [5]. The fiber connections consist of multiple cross-connects at the patch panel between the nodes, and connections to and within the Polatis switch. The capacity estimates are derived mainly using "pure" fiber models. These connections incur

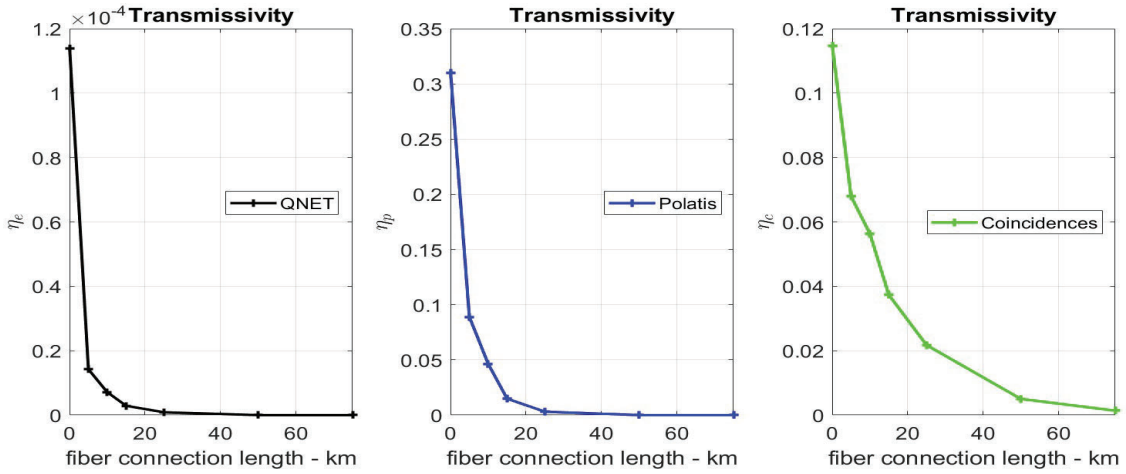

(a) Three estimates based on QNET, Polatis and coincidences measurements, left to right

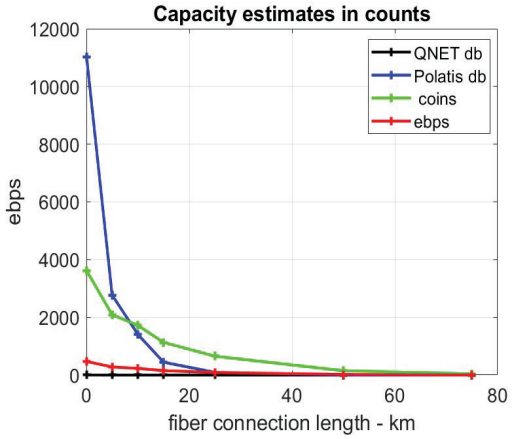

(b) Composite of three estimates

Fig. 5: Transmissivity estimate based on measured coincidence rates is the ratio of coincidence rate connections and loop-back at node Alice, and QNET and Polatis estimates are fractions estimated using connection losses: (a) three estimates based on QNET, Polatis and coincidence rate measurements left to right, and (b) composite of three estimates.

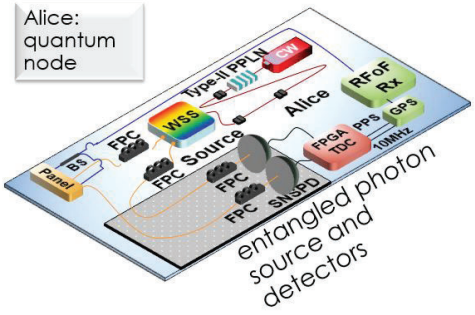

Fig. 6: Two SNSPDs are locally connected to the entangled photon source for coincidence measurements to estimate the source emission rate.

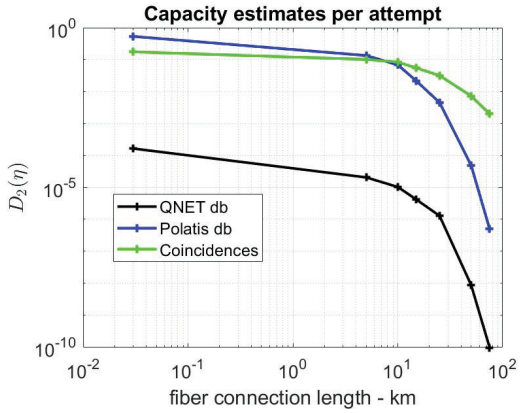

Fig. 7: $D_2(\eta)$ estimates based on transmissivity estimated using coincidence measurements (η_c), Polatis and end-to-end QNET light level measurements, η_p and η_e, respectively.

additional fixed losses that affect both ebps measurements and light levels, and we assume they play a secondary role particularly at longer connection lengths.

B. Transmissivity using Light Levels

For comparison, we approximate η as a fraction of the power that passed through a connection by converting its loss (measured in dB) into a fraction and subtracting from 1, as shown in Fig. 5. This use of the connection power level transmission to approximate the transmissivity η involves the following approximations:

- QNET measurements utilize spectral filtering and calibration for 1560-nm entangled photons, and represent a bulk quantity that includes singles and entangled photons. The assumption is that the losses are not selective to either, and are representative of the entangled ones.
- Polatis measurements correspond to a broader spectrum than those in QNET measurements and have a coarser resolution with no spectral filtering and calibration. The assumption is that these losses are somewhat uniform around the entangled photon transmission bandwidth.

This estimation is approximate since the measured power level includes other components, particularly on the all-optical switch where no spectral filtering and calibration are performed. Using QNET and Polatis measurements, we approximate η_e and η_p, respectively, for end-to-end and partial Polatis paths. The corresponding $D_2(\eta), \eta = \eta_c, \eta_e, \eta_p$ along with those based on coincidence measurements are shown in Fig. 7. The p-capacity based on η_p corresponds to a shorter connection made up of only fiber spools, whereas the e-capacity based on η_e includes connections between Alice and Dave. The difference between them is evident in a lower capacity estimate of the longer connections as shown in Fig. 7. The capacity estimates are derived mainly by treating the connections as entirely composed of fiber as in [5] without explicitly accounting for patching and switching.

V. Measurements and Capacity Estimates

For ebps, the corresponding capacity estimates are given by $S_e D_2(\eta_c)$, where η_c is the transmissivity estimated using coincidence measurements, and S_e is the source rate, as shown in Fig. 8. Additionally, we consider capacity estimates based on η_p using Polatis measurements which correspond to smaller connection losses by about 12.22 dB, and η_e based on end-to-end QNET light level measurements. Both ebps measurements and the corresponding capacity estimates decrease rapidly with distance in Fig. 8, in particular, faster than linear with convex shape which is similar to TCP profile under severe bottlenecks [10]. The ebps measurements are higher than the capacity estimates using light measurements as shown in Fig. 8. On the other hand, the capacity estimates based on η_c are consistent with ebps measurements as they upper-bound the latter for all connections.

The misalignment of capacity estimates using light intensity measurements indicates the importance of choices of measurements needed for analytical methods. When we use the Polatis to measure over artificially shortened connections, that is, these estimates are higher for short distances but decrease to lower values, as shown in Fig. 8. Historically, such considerations

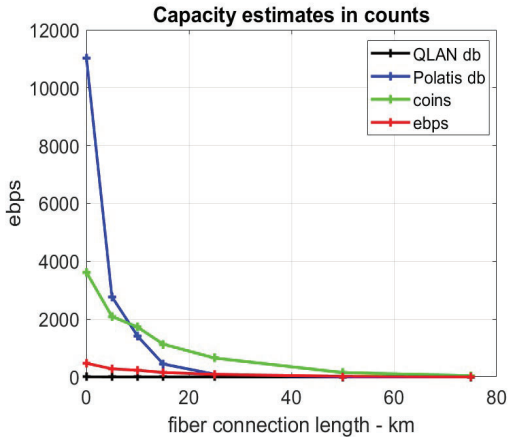

(a) Ebps and capacity in log-log plots

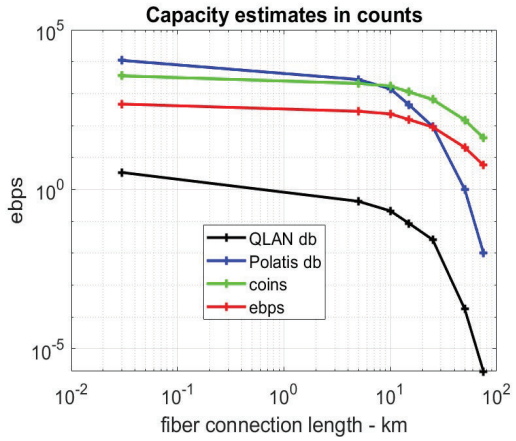

(b) Ebps and capacity log-log plots

Fig. 8: The ebps measurements are below capacity estimates based on coincidence measurements but are higher than capacity estimates based on light level measurements collected on the Polatis switch and QNET Alice node (a) ebps measurements and capacity estimates on a linear scale, and (b) ebps measurements and capacity estimates on a log-log scale.

have been important in the use of the Shannon limit [11] in estimating the capacity of classical networks to correlate measurements with theoretical estimates.

VI. Conclusions

The complementary properties and insights from physical entanglement throughput measurements and the corresponding analytical capacity estimates can play an important role in the development of quantum networks. As a continuation of efforts in that direction, we utilize single photon and power level measurements over a suite of 0-75km optical connections provisioned on QNET testbed. The single channel use capacity estimates are derived using the transmissivity estimates based on two-photon coincidence measurements. Then, the corresponding capacity bounds on ebps are derived using a multiplier derived from co-located detectors measurements, which are consistent. A comparison with capacity estimates using

light measurements indicates the need for a close alignment of measurements and analytical estimates, and provides insights for this work at the intersection of experimental and analytical methods.

In the important area of throughput estimation in quantum networks, this work constitutes only an initial step towards reducing the gap between the extensive theory and experiments that have been studied indepth albeit in their own independent ways. Future investigation and refinement are needed for identifying and utilizing measurements and analytical capacity estimation methods for various quantum network throughput metrics. The ebps and its capacity estimates both decay faster than linear with connection length, which is in sharp contrast with concave profiles of TCP bps measurements that decrease slower than linear [10]. TCP employs buffers and loss recovery in sustaining bps throughput, and the exploration of analogous mechanisms for quantum connections are planned for the future.

VII. Acknowledgments

Authors acknowledge the constructive and critical feedback from the anonymous reviewers that significantly improved the presentation of results in this paper. This research was performed in part at Oak Ridge National Laboratory, managed by UT-Battelle, LLC, for the U.S. Department of Energy under contract no. DE-AC05-00OR22725. U.S. Department of Energy, Office of Science, Advanced Scientific Computing Research, under the Entanglement Management and Control in Transparent Optical Quantum Networks, PiQSci: Performance Integrated Quantum Scalable Internet, and Early Career Research projects (Field Work Proposals ERKJ378, ERKJ432, and ERKJ353).

References

[1] J. Schmid, A. Höss, and B. W. Schuller, "A survey on client throughput prediction algorithms in wired and wireless networks," *ACM Comput. Surv.*, vol. 54, no. 9, p. 194, 2021.

[2] J. Alnas, M. Alshowkan, N. S. V. Rao, N. A. Peters, and J. M. Lukens, "Optimal resource allocation for flexible-grid entanglement distribution networks," *Opt. Express*, vol. 30, no. 14, pp. 24 375–24 393, 2022. [Online]. Available: https://opg.optica.org/oe/abstract.cfm?URI=oe-30-14-24375

[3] M. M. Wilde, *Quantum Information Theory*, 2nd ed. Cambridge University Press, 2017.

[4] M. Alshowkan, P. G. Evans, B. P. Williams, N. S. V. Rao, C. E. Marvinney, Y.-Y. Pai, B. J. Lawrie, N. A. Peters, and J. M. Lukens, "Advanced architectures for high-performance quantum networking," *J. Opt. Commun. Netw.*, vol. 14, no. 6, pp. 493–499, 2022. [Online]. Available: http://opg.optica.org/jocn/abstract.cfm?URI=jocn-14-6-493

[5] S. Pirandola, R. Laurenza, C. Ottaviani, and L. Banchi, "Fundamental limits of repeaterless quantum communications," *Nat. Commun.*, vol. 8, p. 15043, 2017. [Online]. Available: https://doi.org/10.1038/ncomms15043

[6] M. Alshowkan, N. S. V. Rao, J. C. Chapman, B. P. Williams, P. G. Evans, R. C. Pooser, J. M. Lukens, and N. A. Peters, "Lessons learned on the interface between quantum and conventional networking," in *Driving Scientific and Engineering Discoveries Through the Integration of Experiment, Big Data, and Modeling and Simulation*, J. Nichols, A. B. Maccabe, J. Nutaro, S. Pophale, P. Devineni, T. Ahearn, and B. Verastegui, Eds. Cham, Switzerland: Springer, 2022, pp. 262–279.

[7] N. S. V. Rao, M. Alshowkan, J. C. Chapman, N. A. Peters, and J. M. Lukens, "Throughput measurements and capacity estimates for quantum connections," in *IEEE INFOCOM 2023 - IEEE Conference on Computer Communications Workshops (INFOCOM WKSHPS)*, 2023, pp. 1–6.

[8] M. Alshowkan, B. P. Williams, P. G. Evans, N. S. Rao, E. M. Simmerman, H.-H. Lu, N. B. Lingaraju, A. M. Weiner, C. E. Marvinney, Y.-Y. Pai, B. J. Lawrie, N. A. Peters, and J. M. Lukens, "Reconfigurable quantum local area network over deployed fiber," *PRX Quantum*, vol. 2, p. 040304, Oct 2021. [Online]. Available: https://link.aps.org/doi/10.1103/PRXQuantum.2.040304

[9] J. C. Chapman, J. M. Lukens, M. Alshowkan, N. Rao, B. T. Kirby, and N. A. Peters, "Coexistent quantum channel characterization using spectrally resolved bayesian quantum process tomography," *Phys. Rev. Appl.*, vol. 19, p. 044026, Apr 2023. [Online]. Available: https://link.aps.org/doi/10.1103/PhysRevApplied.19.044026

[10] N. S. V. Rao, S. Sen, Z. Liu, R. Kettimuthu, and I. Foster, "Learning concave-convex profiles of data transport over dedicated connections," in *Machine Learning for Networking*, E. Renault, P. Muhlethaler, and S. Bourmerdassi, Eds. Lecture Notes in Computer Science 11407, Springer, 2019.

[11] M. Secondini and E. Forestieri, "The limits of the nonlinear shannon limit," in *Optical Fiber Communications Conference and Exhibition (OFC)*, 2016, p. Th3D.1.